communications physics

A Nature Portfolio journal

Article

Article in Press

https://doi.org/10.1038/s42005-026-02829-8

Emergent slowly rotating polarization state suppresses cross beam energy transfer in laser driven fusion plasmas

Check for updates

G. Raj [1] ✉, A. Sunahara [1], T. Cohen[1], S. Gandrothula[1], R. K. Follett [2], P. M. Pattison[1], P. Rudy[1] & S. Nakamura [1]

Cross-beam energy transfer (CBET) between intersecting laser beams remains a major challenge for controlling energy deposition in inertial confinement fusion (ICF) plasmas. Here we show that polarization dynamics can suppress CBET. When two laser beams cross in an inhomogeneous, expanding plasma, the local polarization in the overlap region evolves into a slowly rotating polarization that inhibits stimulated scattering responsible for beam-to-beam energy exchange. We show that this regime can be realized using state-of-the-art lasers with sufficiently narrow bandwidth. Two-dimensional simulations and Stokes-parameter analysis reveal the emergence of a linear slowly rotating polarization (SRP) during the interaction. The mechanism operates for both side and back scattering CBET geometries and remains effective at intensities relevant to modern fusion-class laser systems, providing a route to control laser-plasma coupling in direct-drive ICF.

Precise characterization and engineering of the laser polarization state during multibeam laser-plasma interactions are pivotal for the design of photonic devices such as laser-plasma based polarizers and wave plates[1–3], laser beam smoothing techniques such as the polarization smoothing (PS)[4–8] for reducing the laser plasma instabilities LPIs such as the stimulated Brillouin scattering (SBS) seeded from noise and CBET (SBS seeded from another coherent beam) which are severely detrimental for high gains in both direct and indirect drive ICF experiments at the OMEGA laser facility[9] and the national ignition facility (NIF)[10] respectively.

Suppressing CBET is critical for direct-drive ICF ignition, as CBET losses tightly constrain the design space for future high gain commercially viable inertial fusion energy (IFE)[11–13] reactors. Multiple mitigation strategies, for e.g., partial CBET suppression and enhanced laser absorption have been demonstrated between the crossing beams, with a modest frequency detuning (±2.3Å UV) in experiments on NIF and on-target wavelength shifts of upto $\Delta\lambda \sim 10$ Å on OMEGA laser facilities[14–16]. Further, recent studies have demonstrated that a broadband laser (wavelength $\lambda_0 = 351nm$), with a bandwidth of ≈8 THz ($\Delta\omega/\omega_0 \approx 1\%$ where $\Delta\omega/2\pi$ and $\omega_0 = 2\pi c/\lambda_0$ are the laser bandwidth and angular frequency, respectively) can completely suppress CBET[15,17–20]. Since, such large bandwidths exceed current ICF class laser capabilities, experiments instead combine modest frequency detuning with beam smoothing techniques (introducing spatial and temporal incoherence between the laser beams and the plasma) using spectral dispersion SSD[21–23], random phase plates[24–27] and PS for LPI mitigation.

In PS, a prismatic birefringent KDP (potassium dihydrogen phosphate) crystal splits the beam into two orthogonal polarization states with a small angular separation, generating uncorrelated speckle patterns and thereby weakening the coherent coupling between them, which in turn lowers the laser reflectivity due to the back SBS[8]. Further, studies show that mutually orthogonal, linearly polarized (LP) pump-probe beams crossing at arbitrary angles can tune the probe's polarization state from elliptical (while propagating in ICF targets) to circular, producing PS like effect and suppressing CBET[1–3]. For polarization rotation introduced at the laser source, Barth and Fisch[28] were the first to demonstrate, through analytical theory and one-dimensional (1d) particle-in-cell (PIC) simulations, that for the single beam back SBS, if the incident laser beam linear polarization is rotated with a frequency of the order of the instability growth rate, there is a significant reduction in the overall reflectivity given by a factor $R/R_0 \approx e^{-0.36\Gamma_0'}R_0$, where R_0 is the reflectivity without polarization rotation, Γ_0' is the number of effective e-foldings, provided the system is in the linear regime i.e., $R_0 << 1$. The concept was subsequently extended to single-beam stimulated Raman scattering (SRS) in the highly nonlinear regime using 1D PIC simulations, where a similar suppression of the instability was observed[29]. A related mechanism based on Faraday rotation induced polarization evolution in externally magnetized plasmas was shown to reduce SRS growth[30]. Numerical studies based on a proposed sunlight-like laser possessing a continuous broad frequency spectrum, random phase, and random polarization showed that a laser bandwidth of ≈1% can increase the SRS threshold by about a factor of two through disruption of coherent

[1]Blue Laser Fusion, Goleta, CA, USA. [2]Laboratory for Laser Energetics, University of Rochester, Rochester, NY, USA. ✉e-mail: graj@bluelaserfusion.com

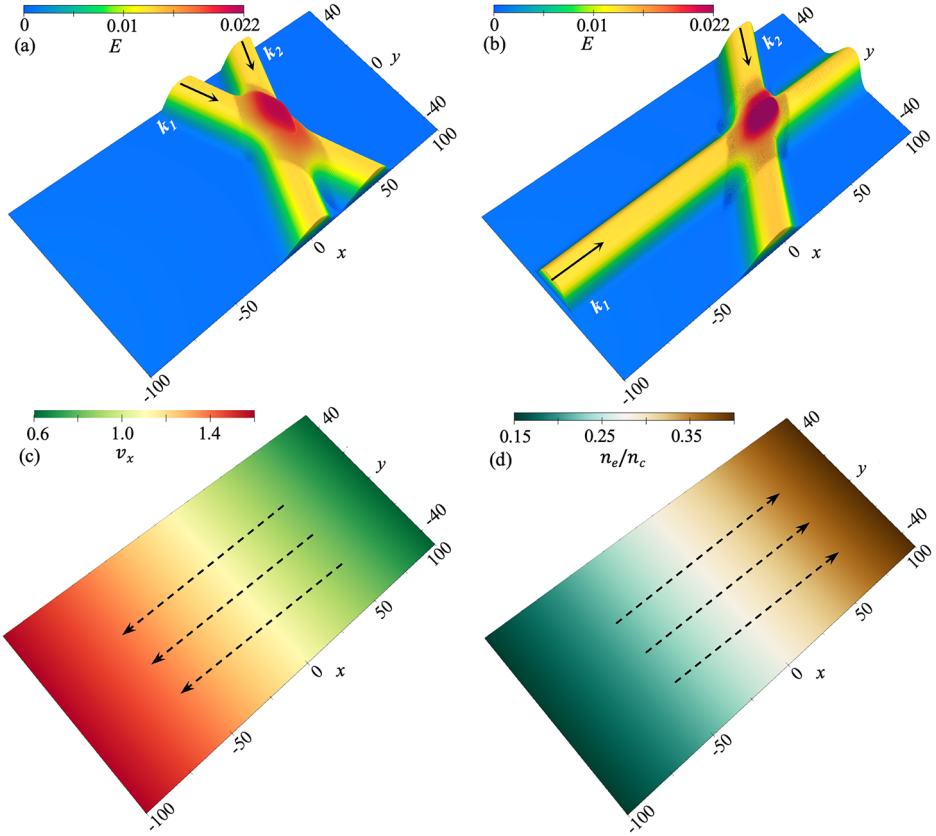

Fig. 1 | Simulation setup. crossing of two CRCP laser beams at 45° with propagation vectors $\mathbf{k_1}$ and $\mathbf{k_2}$ in vacuum (plasma off) for **a** side and **b** back scatter CBET configurations. When the plasma is switched on, **c**, **d** show the simulation domain, where the dashed arrows indicate the directions of the plasma flow velocity ($\boldsymbol{v}_x$) and the density (n_e/n_c) gradients, respectively.

three-wave coupling, while subsequent theoretical work proposed quasi-broadband multi-color laser architectures to realize similar broadband and polarization-randomized conditions in practical high-power laser systems[31,32]. In PS, a prismatic birefringent KDP (potassium dihydrogen phosphate) crystal splits the beam into two orthogonal polarization states with a small angular separation, generating uncorrelated speckle patterns and thereby weakening the coherent coupling between them, which in turn lowers the laser reflectivity due to the back SBS[8]. Further, studies show that mutually orthogonal, LP pump-probe beams crossing at arbitrary angles can tune the probe's polarization state from elliptical (while propagating in ICF targets) to circular, producing PS like effect and suppressing CBET[1–3]. For polarization rotation introduced at the laser source, Barth and Fisch[28] were the first to demonstrate, through analytical theory and one-dimensional (1d) PIC simulations, that for the single beam back SBS, if the incident laser beam linear polarization is rotated with a frequency of the order of the instability growth rate, there is a significant reduction in the overall reflectivity given by a factor $R/R_0 \approx e^{-0.36\Gamma_0'}R_0$, where R_0 is the reflectivity without polarization rotation, Γ_0' is the number of effective e-foldings, provided the system is in the linear regime i.e., $R_0 << 1$. The concept was subsequently extended to single-beam stimulated Raman scattering (SRS) in the highly nonlinear regime using 1d PIC simulations, where a similar suppression of the instability was observed[29]. A related mechanism based on Faraday rotation induced polarization evolution in externally magnetized plasmas was shown to reduce SRS growth[30]. Numerical studies based on a proposed sunlight-like laser possessing a continuous broad frequency spectrum, random phase, and random polarization showed that a laser bandwidth of ≈1% can increase the SRS threshold by about a factor of two through disruption of coherent three-wave coupling, while subsequent theoretical work proposed quasi-broadband multi-color laser architectures to realize similar broadband and polarization-randomized conditions in practical high-power laser systems[31,32].

In this paper, using a approach we show that by using two frequency shifted, counter-rotating circularly polarized (CRCP) lasers interacting at an angle in the direct-drive ICF corona plasma, SRP states can emerge self-consistently in the region of overlap between the two beams. Using 2d simulations with realistic plasma density and flow profiles representative of direct-drive ICF conditions, we show that the emergent SRP states can mitigate multi-beam CBET in both side (Fig. 1a) and back (Fig. 1b) scattering schemes. Unlike previous approaches that relied on polarization rotation introduced at the laser source, external magnetic fields, broadband lasers, or polarization randomization schemes, the SRP state investigated here is generated in situ within the overlap region of two frequency-shifted, CRCP laser beams propagating in an inhomogeneous plasma. Effective CBET mitigation is achieved using only modest frequency offsets between the crossing beams, without requiring multi-THz laser bandwidths or external polarization control. These results identify in situ generated SRP states as an important mechanism for CBET mitigation. At Blue Laser Fusion (BLF), we are developing a new continuous-wave (CW) laser architecture[13], inspired by LIGO[33,34], that combines coherent beam combining (CBC)[35] with an optical enhancement cavity (OEC)[36]. The CBC–OEC platform can provide efficient, cost-effective megajoule-class operation at up to 10 Hz, delivering ≈1–10 kJ per OEC module and aggregating 500–5000 modules to yield a ~5 MJ-class fusion driver. Operating in the UV–visible (λ_0 = 0.35–0.53 μm) with multi-beam wavelength offsets, the CBC–OEC system can result in a total relative bandwidth $\Delta\omega/\omega_0 = \Delta\lambda/\lambda_0$ ~ 1.9% [13], which is comparable to the currently operational FLUX[37] and the proposed sunlight-like laser systems[31,32].

Results

Generation of SRP state

In vacuum, two collinear (θ = 0°) frequency shifted CRCP laser beams propagating along y direction, with right ($\mathbf{E}_+$) and left ($\mathbf{E}_-$) circularly polarized fields, combine to produce a rotating polarization beam with electric field:

$$\begin{aligned}\mathbf{E}(t') &= \mathbf{E}_+(t') + \mathbf{E}_-(t') \\ &= (E_0/2)[\hat{\mathbf{e}}_- e^{-i\omega_1 t'} + \hat{\mathbf{e}}_+ e^{-i\omega_2 t'}] + \text{c.c.}\end{aligned} \quad (1)$$

where $t' = t - y/c, x$ and z are the transverse directions (hereafter subscript x, y, z will denote components along the same directions), $\hat{\mathbf{e}}_{\pm} = \hat{\mathbf{x}} \pm i\hat{\mathbf{z}}, \omega_{1,2} = \omega_0 \pm \Omega$ with Ω as the frequency shift, and E_0 is the peak electric field amplitude[28]. While Eq. (1) is used only to illustrate the basic SRP generation mechanism, the simulations treat the full non-collinear geometry in which the beams cross at 45°, with the resulting SRP state forming self-consistently in the beam overlap region and verified below through the Stokes-parameter analysis. As shown in Fig. 1, in the present scheme we simulate two such CRCP beams with equal intensities, $I_1 = I_2 = 2.0 \times 10^{15}$ W/cm^2; however, they now cross at an angle $\theta \approx 45°$ in two different configurations w.r.t. the direction of the plasma density gradient and the flow. For central laser frequency $\omega_0 = 5.37 \times 10^{15}$rad/s ($\lambda_1 = 351$ nm), and $\Omega = 3.14 \times 10^{12}$ rad/s the beams have an individual bandwidths of $\Delta\omega/\omega_{1,2} \approx 0.06\%$. Since both CBET and SBS are mediated by ion-acoustic waves, we choose $\Omega = 3.14 \times 10^{12}$, rad/s following the rotating polarization suppression criterion derived for SBS by Barth and Fisch[28]. Using the multi-dimensional wave based laser plasma simulation environment (LPSE) code, developed at the laboratory for laser energetics (LLE), Rochester[38,39], Fig. 1 shows the absolute square of the electric field, $E\,(= 2[e/m_e c\omega_0]^2\langle|\mathbf{E}(t')|^2\rangle_{2\pi/\omega_0})$, in vacuum. The code efficiently models multi-beam, non-paraxial propagation in expanding, inhomogeneous, time-dependent plasmas relevant to direct-drive ICF.

The 2d simulation domain in Fig. 1 has dimensions $L_x = 200$ μm and $L_y = 100$ μm with cell size $\Delta L_x = \Delta L_y = 50$ nm, and is filled with CH plasma having electron and ion temperatures $T_e = 3$ keV and $T_i = 1$ keV, respectively. Plasma expansion results in a linearly varying plasma sonic flow velocity $\mathbf{v}_x$ (Fig. 1c) and electron density profile $n_e(x)/n_c$ (Fig. 1d) from $[x, \mathbf{v}_x, n_e] = [-100\ \mu\text{m}, 1.6\ M, 0.15\ n_c]$ to $[+100\ \mu\text{m}, 0.6\ M, 0.4\ n_c]$, where $n_e(x) = m_e\omega_{pe}^2(x)/4\pi e^2$ is the plasma electron density, m_e and e are the rest mass and charge of an election respectively, $n_c\,(= m_e\omega_0^2/4\pi e^2)$ is the critical plasma density. Fixing $\mathbf{v}_x$ and n_e uniform along y direction, yields an interaction length $L_n \simeq 200$ μm, which is consistent with direct-drive OMEGA[19,38] experiments. Collisional absorption is disabled, and the ion-acoustic wave (IAW) is damped by electron Landau damping at a constant rate $\nu_a = 0.14\, k_a c_s$, approximating collisionless IAW damping in CH[19,40] plasma, where $c_s = \left[(Zk_BT_e + 3k_BT_i)/m_i\right]^{1/2}$, Z is the ion charge, and k_B is Boltzmann's constant.

Role of SRP in CBET suppression

In Fig. 2, for typical values of high (Fig. 2a–d) and low (Fig. 2e–h) intensity laser beams used in different direct drive ICF schemes, at the end of 4 ps, we investigate CBET between crossing CRCP and LP by introducing the CH plasma in the simulation setup of Fig. 1. Since SBS is a resonant three wave process where a pump (subscript 1) laser scatters into a second frequency downshifted electromagnetic (*e.m.*) probe wave (subscript 2) and an IAW, they satisfy the matching condition $\mathcal{R} \equiv (\omega_1 - \omega_2) - (\mathbf{k}_1 - \mathbf{k}_2)\cdot\mathbf{v} - |\mathbf{k}_1 - \mathbf{k}_2|c_s = 0$, where $\mathbf{v}$ is the plasma flow velocity. In case of stationary plasma ($|\mathbf{v}| = 0$ in $\mathcal{R}$), the two *e.m.* waves must be frequency detuned so that their beat frequency matches the finite IAW frequency, satisfying the energy ($\hbar\omega_1 = \hbar[\omega_2 + \omega_{\text{IAW}}]$, where $\omega_{\text{IAW}} = k_{\text{IAW}}c_s$ is the IAW frequency) and momentum ($\hbar\mathbf{k}_1 = \hbar[\mathbf{k}_2 + \mathbf{k}_{\text{IAW}}]$) matching conditions. However, in the present study which considers an inhomogeneous, expanding plasma with $\omega_1 = \omega_2$, the matching condition is satisfied with an appropriate combination of flow (around $\mathbf{v} \approx 1$ Mach region) and pump-probe frequency shift between the CRCP and LP lasers crossing in the plasma.

For the high intensity case using (LP) beams, Fig. 2a shows that the back scattering CBET is very strong with ≈90% of beam 1 reflecting back into beam 2, however for the same lasers the side scattering CBET is slightly less at ≈77% as observed in Fig. 2c. Replacing the two LP beams in Fig. 2a, c with the same intensity, CRCP laser beams as in Fig. 2b, d, significantly reduces CBET to ≈8% and ≈1.5%, respectively. Similarly, a complete CBET suppression is observed in the case of low intensity laser beams with the two CRCP (Fig. 2f, h) beams as compared to the LP (Fig. 2e, g) beams, for which CBET from beam 1 to 2 is ≈33% and 30%, respectively for the back (Fig. 2e) and side (Fig. 2g) scattering CBET configurations.

Stokes-Poincaré sphere dynamics of SRP

Using Eq. (1), we can define Stokes parameters[41] as $S_0 = |E_{0x}|^2 + |E_{0z}|^2$, $S_1 = |E_{0x}|^2 - |E_{0z}|^2$, $S_2 = 2\,\Re\left(E_{0x}E_{0z}^*\right)$, and $S_3 = -2\,\Im\left(E_{0x}E_{0z}^*\right)$, where E_{0x} and E_{0z} are complex amplitudes of E_0. The position of normalized Stokes vector $\mathbf{s}(t) = (s_1, s_2, s_3) = (S_1, S_2, S_3)/S_0$, on the unit Poincaré sphere ($|\mathbf{s}| = 1$ for fully polarized laser light)[42] along with its orientation (ψ) and ellipticity (χ) angles defined in Eqs. (2a) and (2b) respectively below

$$\psi(t) = (1/2)\arctan 2(S_2, S_1) \in [-\pi/2, +\pi/2], \tag{2a}$$

$$\chi(t) = (1/2)\arcsin(S_3/S_0) \quad \in [-\pi/4, +\pi/4], \tag{2b}$$

can reveal the different states of laser polarization as shown in Fig. 3a. To verify the occurrence and significance of the SRP state during CBET suppression, we analyze the high intensity CRCP case ($I_0 = I_1 = 2.0 \times 10^{15}$ W/cm^2) shown in Fig. 2a–d. From the three components of the complex field amplitudes sampled at the center of the beam overlap region (where $\mathbf{v} \approx 1$ Mach) in both side and back scattering CBET geometries, we compute and plot the time evolution of the normalized Stokes vector $\mathbf{s}(t)$ in Fig. 3b, e along the bisector between the crossing beams. Fig. 3e shows that, for side-scattered CBET suppression with CRCP laser [cf. Fig. 2d] case, the Stokes vector $\mathbf{s}(t)$ traces a narrow, closed orbit (yellow solid curve) on the Poincaré sphere near the equator (transiting through all LP states; cf. Fig. 3a), demonstrating predominantly a coherent slowly rotating linear polarization (SRLP) state. In contrast, Fig. 3d shows that in case of strong side CBET with the LP lasers [cf. Fig. 2c], the $\mathbf{s}(t)$ is essentially stationary in time (yellow dot), indicating no polarization rotation.

The SRLP state in Fig. 3e is consistent with Fig. 4a, where the dashed curve shows the normalized Stokes orientation angle $\psi(t)$ increasing almost linearly in time, implying an approximately constant polarization rotation rate. Note that the step changes in the sawtooth evolution of $\psi(t)$ are a plotting artifact: the polarization pattern repeats after a rotation by π, so ψ is displayed within the fixed angle range of Eq. (2a). The rotation rate $\Omega_{\text{rot}} = \Delta\psi/\Delta t$ is obtained from the slope of the linear sawtooth ramp segments in Fig. 4a for the side-scattering CBET (dashed curve) case, with $\Delta\psi = \pi$ and $\Delta t = 1$ps, giving $\Omega_{\text{rot}} = 3.1 \times 10^{12}$rad/s, i.e., many orders of magnitude slower than the optical frequency. The dashed curve in Fig. 4b further shows that the ellipticity $\chi(t)$ remains small, $|\chi| \lesssim 6 \times 10^{-2}$rad, confirming that the trajectory stays near the linear-polarization equator ($s_3 \simeq 0$) and that the slow rotation is accompanied only by weak periodic ellipticity modulation for the side-scattering CBET.

For back-scattered CBET attenuation [cf. Fig. 2b] with CRCP lasers, the yellow solid curve in Fig. 3c shows that after a brief initial transient excursion, the Poincaré-sphere trajectory of the normalized Stokes vector $\mathbf{s}(t)$ locks onto a steady near-equatorial closed orbit, consistent with an SRLP state. This is corroborated by the orientation angle $\psi(t)$ (solid curve) in Fig. 4a: after a short transient ($\lesssim$1 ps), $\psi(t)$ becomes highly regular and exhibits a sawtooth pattern analogous to the side-scattered CRCP case (dashed curve), yielding a similar rotation rate Ω_{rot}. The ellipticity angle $\chi(t)$ (solid curve) in Fig. 4b remains small ($|\chi| \lesssim 10^{-1}$rad) but shows a systematic negative bias and periodic excursions.

Notably, the strong CBET suppression for the CRCP case w.r.t. LP can be attributed to slowly rotating (oscillating) polarization in the overlap region, which reduces the effective pump-plasma interaction length[28]. This can be demonstrated using the phase-matching condition $\mathcal{R} \equiv (\omega_1 - \omega_2) - \mathbf{k}_{\text{IAW}}\cdot\mathbf{v} - k_{\text{IAW}}\,c_s = 0$, where $\mathbf{k}_{\text{IAW}} \equiv \mathbf{k}_1 - \mathbf{k}_2$ and $k_{\text{IAW}} \equiv |\mathbf{k}_{\text{IAW}}|$. For LP beams $\omega_1 = \omega_2$, $\mathcal{R}_{\text{LP}} = 0$ is satisfied where $\mathbf{k}_{\text{IAW}}\cdot\mathbf{v} = -\,k_{\text{IAW}}\,c_s$, i.e., where the flow Doppler-shifts the IAW into resonance with the ponderomotive beat, driving the strong IAW coherently over L_n with e-folding $\Gamma_0' = \gamma_0 L_n/c$, where γ_0 is the growth rate for co-polarized LP beams, (Eq. (21) in ref. 28, adapted for present geometry) resulting in strong CBET. For CRCP beams case since $\omega_{1,2} = \omega_0 \pm \Omega$,

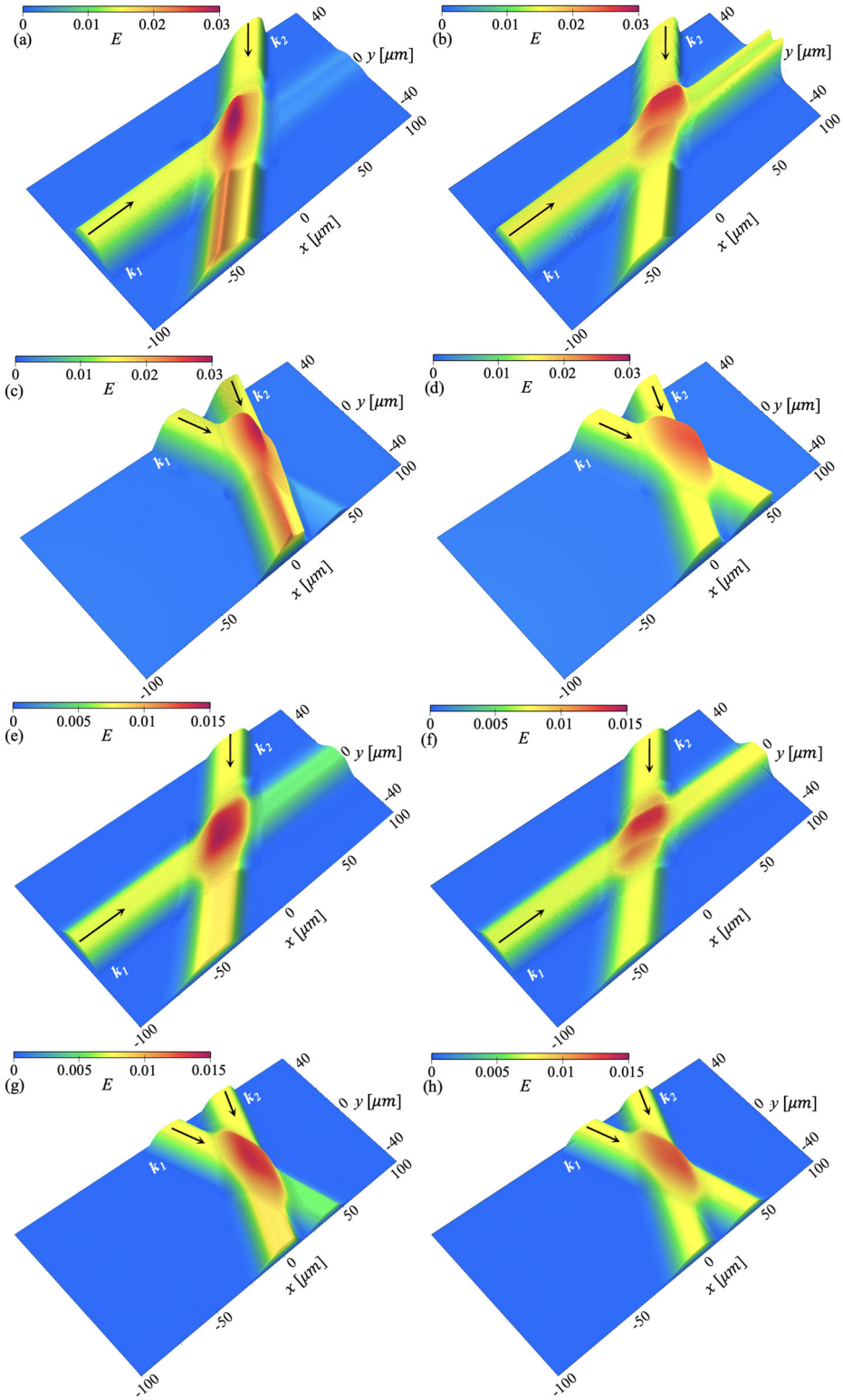

Fig. 2 | CBET suppression by slowly rotating polarization at high and low laser intensity. Snapshots at $t = 4$ ps showing CBET for **a**–**d** high intensity ($I_1 = I_2 = 2.0 \times 10^{15}$ W/cm^2) and **e**–**h** low intensity ($I_1 = I_2 = 5.0 \times 10^{14}$ W/cm^2) laser beams with LP and CRCP in the left and right panels, respectively for each case, where all the top and bottom panels are for back and side scattering cases, respectively. The beam overlap regions for the back and side CBET cases are $[x, \mathbf{v}_x, n_e]_{\text{back}} = [-30\,\mu\text{m},\ 1.25M,\ 0.22n_c]$ to $[+30\,\mu\text{m}, 0.95M, 0.31n_c]$ and $[x, \mathbf{v}_x, n_e]_{\text{side}} = [2\,\mu\text{m},\ 1.1M,\ 0.27n_c]$ to $[+\,35\,\mu\text{m},\ 0.92M, 0.32n_c]$, with transverse extents $y = [-12, +12]\,\mu$m and $y = [-35, +35]\,\mu$m, respectively. For the LP laser side and back scatter cases, the two beams are p and s polarized, respectively.

$\mathcal{R}_{\text{CRCP}} = 2\Omega_{\text{rot}} \neq 0$, this shifts the ponderomotive beat frequency off the IAW resonance by $2\Omega_{\text{rot}}$. Consequently, for SRP this detuning results in a time-dependent growth rate (ref. 28, Eq. (20)) given by $\gamma(t) = \gamma_0 p_c$, where $p_c = |\cos(\Omega_{\text{rot}} t)|$ is the polarization coupling with $p_c = 1$ for co-polarized LP beams. For the such LP beams p_c is independent of time, thus satisfying the condition $\mathcal{R} = 0$ at all times and gaining the full e-folding Γ_0' over L_n. However, for the SRP case, Fourier decomposition of the time-dependent p_c gives:

$$|\cos(\Omega_{\text{rot}} t)| = \underbrace{\frac{2}{\pi}}_{\substack{\mathcal{R}=0 \\ \text{resonant}}} + \frac{4}{\pi}\sum_{n=1}^{\infty}\frac{(-1)^{n+1}}{4n^2-1}\underbrace{\cos(2n\Omega_{\text{rot}} t)}_{\substack{\mathcal{R}=2n\Omega_{\text{rot}}\neq 0 \\ \text{off}-\text{resonant}}}, \quad (3)$$

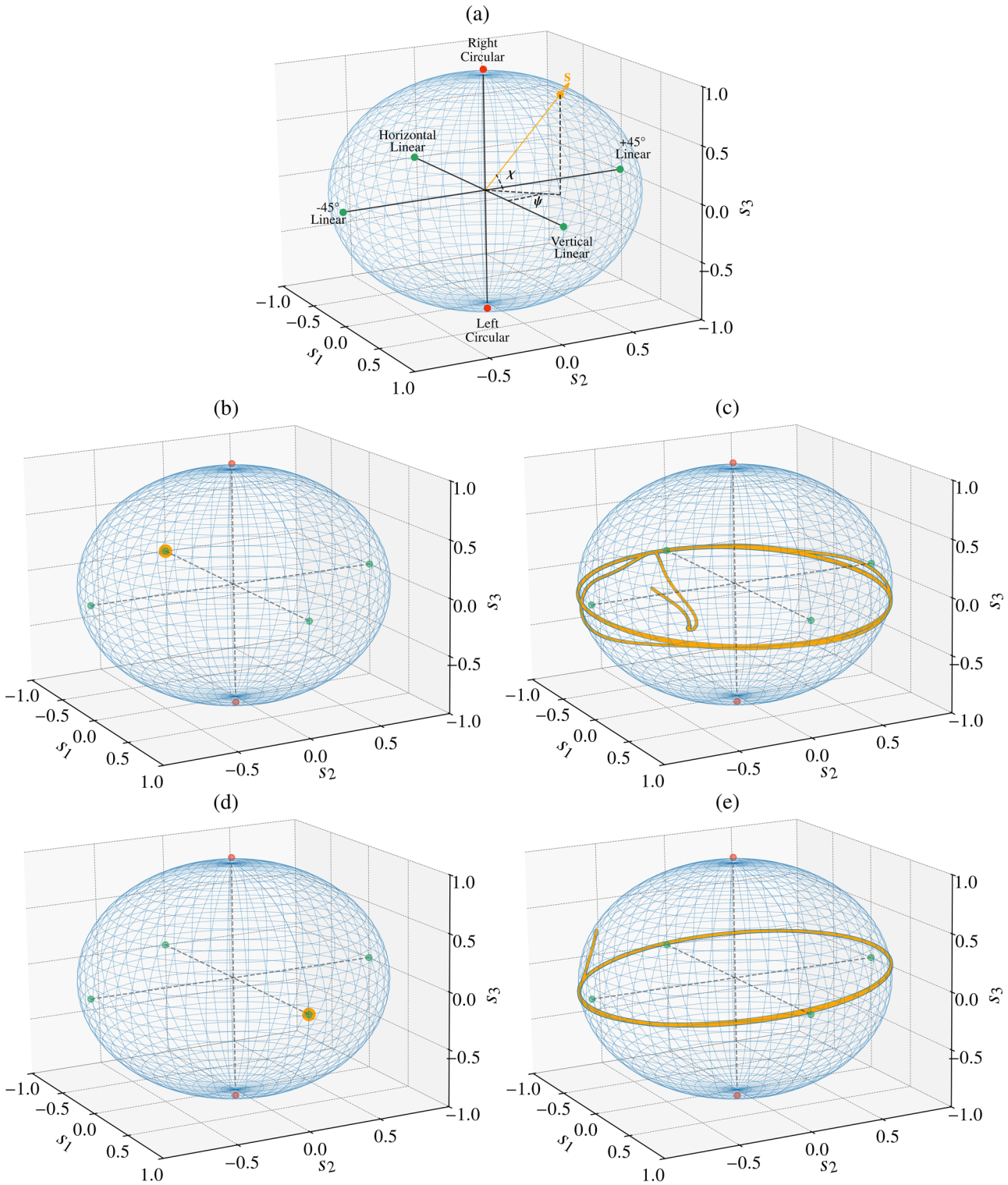

Fig. 3 | Poincaré sphere trajectories of the normalized Stokes vector for linearly and circularly polarized beams. a Laser polarization states represented by the position of Stokes vector $\mathbf{s}(t)$ on the Poincaré sphere. Time traces of $\mathbf{s}(t)$ from the simulations in Fig. 2: for **b** linearly polarized (LP) back (cf. Fig. 2a); **c** counter-rotating circularly polarized CRCP back (cf. Fig. 2b); **d** LP side (cf. Fig. 2c); and **e** CRCP side (cf. Fig. 2d) scattering CBET configurations.

where only the time-independent component ($2/\pi < 1$) satisfies $\mathcal{R} = 0$ and drives a weakly resonant IAW, while the remaining oscillating terms at $\mathcal{R} = 2n\Omega_{\rm rot} \neq 0$ do not contribute to CBET. Hence the effective e-folding for the SRP case reduces directly to (Eqs. (21) and (25) in ref. 28) $\Gamma_{\rm SRP} = (2/\pi)\Gamma_0' < \Gamma_0'$, for $\Omega_{\rm rot} \gg 2c/L_n$, directly accounting for the stronger CBET in the LP case (Fig. 2a, c) versus the suppressed CBET in the SRP case (Figs. 2b, d). Complete suppression further requires[28] $(\pi/2\Omega_{rot}) < (1/\gamma_0)$ i.e., $\Omega_{\rm rot} \gtrsim \gamma_0$, satisfied in our simulations, consistent with strong CBET mitigation in Figs. 2b, d, f, h. Further, the local polarization state (via the Stokes parameters) is set by the field amplitudes and their relative phase. The SRLP state in Fig. 3b, c arises from nearly equal amplitudes and a slowly varying phase; however, energy exchange, propagation-induced phase

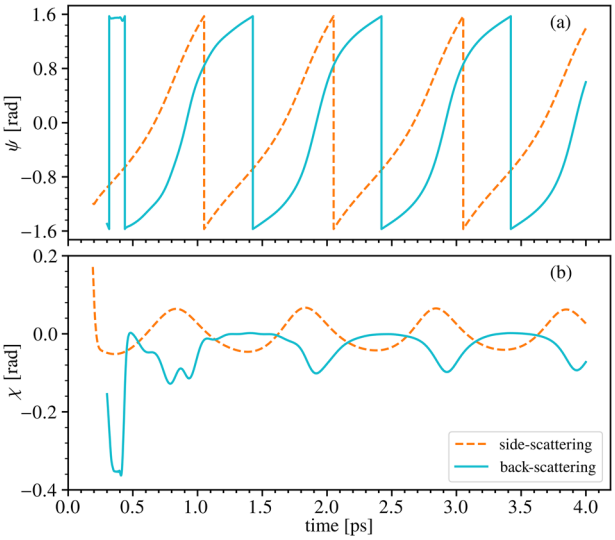

Fig. 4 | Time evolution of the Stokes orientation and ellipticity angles for side and back scattering CBET. For the $I_1 = I_2 = 2.0 \times 10^{15}$ W/cm^2 case in Fig. 2, variations in the orientation $\psi(t)$ (**a**)) and ellipticity $\chi(t)$ (**b**)) of the normalized Stokes vector $\mathbf{s}(t)$ with time, where the dashed and the solid curves correspond to the side and back scattering CBET cases, respectively.

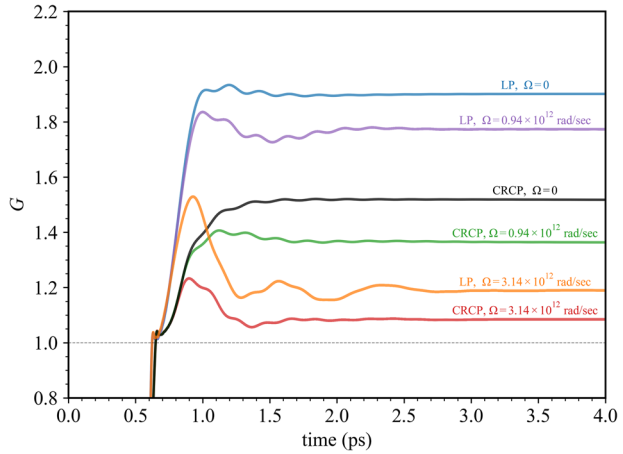

Fig. 5 | CBET induced energy gain for different frequency shifts between LP and CRCP beams. Energy gain (G) for beam 2 in the back-scattered CBET with $I_1 = I_2 = 2.0 \times 10^{15}$ W/cm^2 case in Fig. 2. The energy gain is plotted as a function of time for different frequency shifts between the LP and CRCP beams in back CBET configuration. Larger values of G indicate stronger CBET.

shifts, and plasma-flow Doppler shifts can modulate these parameters, also producing slowly rotating, highly elliptic polarization states in the overlap region.

We note that, the applied frequency shift (Ω) is the discrete separation between the frequencies of the two CRCP beams, rather than a continuous spectral bandwidth. However, for the present analysis, it may be interpreted as an effective two-color bandwidth. To distinguish the SRP induced suppression of CBET from the intrinsic effect of frequency detuning, in Fig. 5, we compare the CBET induced energy gain ($G = E_{out}/E_{in}$) of beam 2 for different Ω for both the LP and CRCP backscatter CBET configurations (important in direct-drive conditions) for $I_1 = I_2 = 2.0 \times 10^{15}$ W/cm^2 case in Fig. 2. Here, E_{in} and E_{out} are the input and output energies of beam 2 recorded at the upstream and downstream boundaries respectively.

Figure 5 shows that CBET saturates at around ≈1–1.25 ps, after which it reaches a nearly steady state. We first compare the two base cases shown in Fig. 2: the LP beams case for $\Omega = 0$ (Fig. 2a) and the CRCP beams (with SRP) case for $\Omega = 3.14 \times 10^{12}$ rad/s (Fig. 2b). The blue curve shows that CBET is strongest for the LP base case, with beam 2 gaining ≈ 90% energy. In contrast, the red curve shows that the gain for the CRCP base case is significantly reduced to only ≈8%. The black curve shows the CRCP case with $\Omega = 0$, where the gain is reduced to ≈ 51% w.r.t. LP base case but still significantly higher w.r. t. CRCP (with SRP) base case, indicating that circular polarization alone does not significantly suppress CBET when there is no polarization rotation. Thus, the strong reduction observed for the base CRCP case arises from the combined effect of frequency shift and polarization rotation, rather than from circular polarization alone.

For the LP beams with the same frequency shift as the CRCP base case, shown by the orange curve, the CBET gain of beam 2 is reduced to ≈20%. However, this is still significantly larger than the gain for the CRCP beams at the same frequency shift (base CRCP case). This comparison shows that frequency shift alone reduces CBET, but in the base CRCP case additional suppression is provided through the SRP. Furthermore, comparing the LP beams and CRCP beams with ≈3.5 smaller frequency shift of $\Omega = 0.94 \times 10^{12}$rad/s w.r.t. the base CRCP case, shown by the magenta and green curves, respectively show that for the LP case gain is ≈75%, whereas for the CRCP case, the gain is reduced to ≈36%. Thus, even when the intrinsic frequency shift effect is weakened, the CRCP configuration still provides additional CBET suppression through SRP, although the CBET suppression is weaker than in the higher frequency shift base CRCP case. We observe similar results for the side-scattered CBET case in Figs. 2c, d. These results confirm that polarization rotation acts as an important CBET suppression mechanism in addition to the frequency detuning effect.

Figure 6a, b, show the normalized IAW density perturbation from the simulations in the beam overlap region at 4 ps for the LP and CRCP cases, respectively, corresponding to the highest laser intensity ($I_1 = I_2 = 2.0 \times 10^{15}$ W/cm^2) cases of Figs. 2a, b. The results show strong IAW density perturbations for the LP case hence strong CBET while for the CRCP case with SRP the IAW density perturbations are significantly reduced (weakly resonant IAW in Eq. (3)) leading to strong CBET suppression. In Fig. 6c we plot the temporal evolution of the normalized peak ($|\delta n/n_0|_{peak}$) IAW density perturbations from the simulations for the two cases in Figure 6a, b. The figure shows that the maximum value of $|\delta n/n_0|_{peak}$ for LP $\simeq 3.0 \times 10^{-2}$ (blue curve) and CRCP $\simeq 9.0 \times 10^{-3}$ (orange curve) cases, implying that $|\delta n/n_0|_{peak} << 1$. Thus, the driven IAW response is in the linearized regime where nonlinear IAW saturation mechanisms, such as ion trapping, wave breaking, or nonlinear frequency shifts, are not expected to dominate. The observed saturation is therefore governed primarily by pump depletion and damping of the driven IAW at a constant rate[19]. This is also consistent with the recent work of Seaton et. al.[43], who compared LPSE and PIC simulations for CBET relevant conditions and found that a fluid linear response with linear Landau damping is adequate when nonlinear kinetic effects are weak.

Conclusions

In conclusion, while Barth and Fisch[28] applied the SRLP to a single incident beam to suppress parametric backscatter, the present work shows that SRLP states can be generated in situ in the overlap region of two crossing CRCP beams in an inhomogeneous, expanding plasma. This SRLP state suppresses the ion-acoustic density grating responsible for CBET. With $\Omega_{rot} \ll \omega_{1,2}$ and $\Omega_{rot} \approx \Omega$ (frequency shift between the CRCP lasers), the SRP states can strongly mitigate CBET at fractional bandwidths ($\Delta\omega/\omega_0 \lesssim 0.15\%$), well below conventional broadband approaches. For LP beams, increasing frequency detuning ($\Delta\omega/\omega_0 \gtrsim 0.15\%$) can in principle yield comparable CBET suppression, consistent with simulation studies in ref. 14, which showed that using broad bandwidth $\Delta\omega/\omega_0 \sim 1\%$ eliminates CBET losses under direct-drive conditions for 351 nm, 16 speckled LP beams at an intensity of 1.5×10^{14} W/cm^2. Using this $\Delta\omega/\omega_0 \sim 1\%$ result as a reference scale (not as a threshold for the present study), at sufficiently large detuning LP suppression may approach the SRP result as CBET becomes strongly suppressed by spectral detuning alone. However, this threshold is laser-plasma parameter

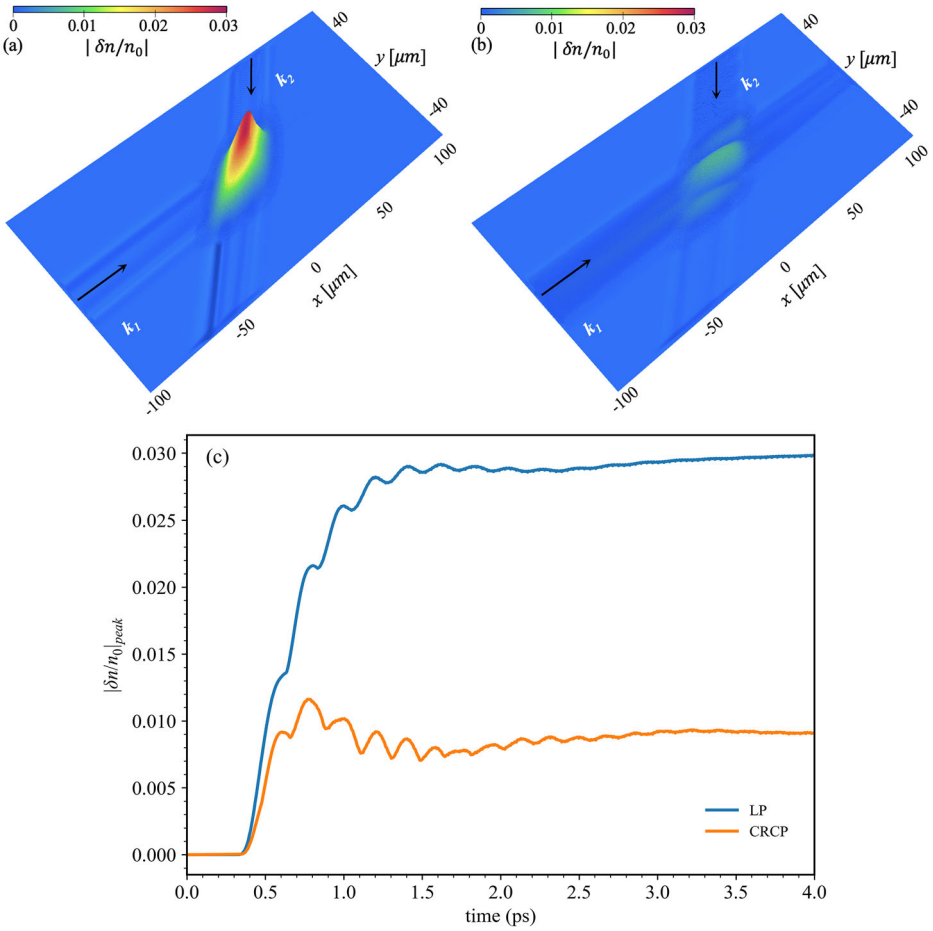

Fig. 6 | Ion-acoustic wave density perturbations for LP and CRCP cases. a, **b** Show snapshots of the normalized IAW density perturbation at 4 ps in the beam overlap region for the LP and CRCP cases, respectively, corresponding to the high-intensity cases of Fig. 2a, b. **c** Shows the temporal evolution of the normalized peak ($|\delta n/n_0|_{peak}$) ion-acoustic density perturbation from the simulations for the two cases.

dependent and may require bandwidths exceeding the fractional bandwidth limit considered in the present study.

Suppression is highly efficient in both back and side scattering CBET configurations, relevant to direct-drive (OMEGA) and indirect-drive (NIF) ICF, respectively. Because the CBET growth rate scales with the crossing beam intensities, this mechanism is particularly important for direct-drive ICF schemes using higher intensity ($I_1 = I_2 \gtrsim 1.0 \times 10^{15}$ W/cm^2) lasers. Further, we separate the effects of frequency detuning from polarization rotation by comparing frequency-shifted LP and CRCP beams at the same imposed frequency shifts. The LP cases isolate detuning effects as compared to the CRCP cases which include both detuning and SRP effects. The study shows that frequency detuned LP beams can alone reduce CBET, but CRCP beams with SRP give stronger suppression under the same conditions. Consistent with the Barth and Fisch[28] results, the suppression of CBET weakens when the frequency shift, and therefore the polarization rotation rate, is reduced. These results show that the mitigation is not simply a bandwidth (frequency shift) effect but also arises from SRP induced reduction of coherent laser IAW coupling.

We also note that frequency shifted LP beams with mutually orthogonal polarizations could also reduce CBET in an idealized two-beam geometry. However, in realistic ICF plasmas and multi-beam configurations, maintaining pairwise polarization orthogonality at each overlap region can be challenging. By contrast, the CRCP configuration provides a more robust way to generate a rotating polarization state through the frequency shift, making the suppression less dependent on strict pairwise polarization alignment. The SRP mechanism is studied here in the context of mitigating CBET, a dominant LPI process in direct-drive ICF. While polarization rotation can reduce backscattering instabilities such as SBS and SRS, its effect on other LPIs may depend on the laser-plasma parameters. A detailed investigation of the effect of SRPs on multi-beam (≫2 beams) CBET, along with its influence on other LPIs is beyond the scope of the present work and will be undertaken in a future study. Thus, using SRP can complement the established LPI control methods leading to effective CBET mitigation which could help enable efficient, high-gain direct-drive IFE reactors in the future.

Methods

LPSE simulation

The 2d simulations were performed using the (LPSE)[38,39], a wave-based fluid, Eulerian simulation code developed to simulate the interaction of multiple laser beams with plasma over large spatial domains. The code occupies the middle ground between two extremes: the fully kinetic PIC[44] or Vlasov codes which resolve individual particle dynamics but are computationally prohibitive at ICF relevant plasma volumes, and the radiation hydrodynamic codes[45], which model the bulk plasma evolution but contain no LPI physics. LPSE solves coupled, temporally enveloped wave equations for the electromagnetic laser fields and plasma perturbations on a fixed Cartesian grid. The plasma response is modeled within the fluid approximation, where the electron plasma wave, and the IAW perturbations are linearized relative to the background plasma density. This framework enables the investigation of key LPIs such as the (SRS), two plasmon decay, resonance absorption (RA) and CBET, thus capturing the collective dynamics of LPIs while remaining computationally efficient for large plasma volumes with prescribed density and flow profiles representative of laser-driven fusion plasmas.

Furthermore, the code employs a non-paraxial, full vector formulation in which all three Cartesian components of the complex electric field envelope (E_{0x}, E_{0y}, E_{0z}) are evolved independently on the 2d spatial plasma grid, preserving all polarization degrees of freedom. This full vector treatment is essential to the present study, as the suppression of CBET via the

emergent SRP state fundamentally depends on the relative polarization state $\hat{\mathbf{e}}_+ \cdot \hat{\mathbf{e}}_-$ of the two crossing beams, which is only correctly captured when all polarization degrees of freedom are retained. Also, it must be noted that the theoretical and numerical work by Barth and Fisch[28], which showed the SRP mechanism for parametric backscattering suppression, was performed using 1d PIC simulations compared to an analytical fluid model estimates. In the present work, we use 2d simulations performed using an independent code (LPSE), in an inhomogeneous, expanding plasma with a realistic density and flow velocity profile relevant to direct-drive ICF. The validity of the SRP suppression mechanism is evidenced by its consistency in going from 1d to 2d across different codes, different plasma geometries, and different instability regimes (single beam SBS in ref. 28 vs two beam CBET now) thus demonstrating that the suppression is an intrinsic physical consequence of the polarization dynamics. Hence, we expect the results to remain valid in 3d, where the IAW grating is subject to additional out of plane damping that is absent in 2d. This would only weaken the baseline CBET further, implying our 2d results provide a conservative lower bound on the SRP suppression efficiency in 3d.

Data availability

The numerical simulation data supporting the findings of this study were generated using the LPSE code and are stored on secure servers at Blue Laser Fusion Inc. Data are available from the corresponding author (G. Raj, graj@bluelaserfusion.com) upon request and subject to permission from the authors' institution, Blue Laser Fusion Inc.

Code availability

The LPSE simulation code used in this study was developed at the Laboratory for Laser Energetics (LLE), University of Rochester, and is distributed under license. The code is not publicly available but may be obtained from the developers subject to institutional licensing agreements.

Received: 18 March 2026; Accepted: 12 August 2026;
Published online: 22 August 2026

References

1. Michel, P., Divol, L., Turnbull, D. & Moody, J. D. Dynamic control of the polarization of intense laser beams via optical wave mixing in plasmas. *Phys. Rev. Lett.* **113**, 205001 (2014).
2. Turnbull, D. et al. High power dynamic polarization control using plasma photonics. *Phys. Rev. Lett.* **116**, 205001 (2016).
3. Turnbull, D. et al. Refractive index seen by a probe beam interacting with a laser-plasma system. *Phys. Rev. Lett.* **118**, 015001 (2017).
4. Epperlein, E. M. in *Lle Review Quarterly Report* Vol. 45 (USDOE, 1990).
5. Lefebvre, E. et al. Reduction of laser self-focusing in plasma by polarization smoothing. *Phys. Plasmas* **5**, 2701–2705 (1998).
6. Skupsky, S. & Craxton, R. S. Irradiation uniformity for high-compression laser-fusion experiments. *Phys. Plasmas* **6**, 2157–2163 (1999).
7. Tsubakimoto, K. et al. Suppression of interference speckles produced by a random phase plate, using a polarization control plate. *Opt. Commun.* **91**, 9–12 (1992).
8. Moreau, J. G. et al. Stimulated brillouin scattering dependence on polarization state, speckle shape, and polarization smoothing implementation. *Phys. Plasmas* **32**, 032102 (2025).
9. Campbell, E. et al. Laser-direct-drive program: Promise, challenge, and path forward. *Matter Radiat. Extrem.* **2**, 37–54 (2017).
10. Moses, E. I., Boyd, R. N., Remington, B. A., Keane, C. J. & Al-Ayat, R. The national ignition facility: ushering in a new age for high energy density science. *Phys. Plasmas* **16**, 041006 (2009).
11. Nuckolls, J., Wood, L., Thiessen, A. & Zimmerman, G. Laser compression of matter to super-high densities: thermonuclear (ctr) applications. *Nature* **239**, 139–142 (1972).
12. Betti, R. & Hurricane, O. A. Inertial-confinement fusion with lasers. *Nat. Phys.* **12**, 435–448 (2016).
13. Sunahara, A. et al. Laser-based inertial fusion energy system enabled by optical enhancement cavities and a direct-drive configuration reactor. *Opt. Express* **33**, 47104–47120 (2025).
14. Bates, J. W. et al. Suppressing parametric instabilities in direct-drive inertial-confinement-fusion plasmas using broadband laser light. *Phys. Plasmas* **30**, 052703 (2023).
15. Edgell, D. H. et al. Mitigation of cross-beam energy transfer in symmetric implosions on Omega using wavelength detuning. *Phys. Plasmas* **24**, 062706 (2017).
16. Marozas, J. A. et al. First observation of cross-beam energy transfer mitigation for direct-drive inertial confinement fusion implosions using wavelength detuning at the National Ignition Facility. *Phys. Rev. Lett.* **120**, 085001 (2018).
17. Bates, J. et al. Suppressing cross-beam energy transfer with broadband lasers. *High. Energy Density Phys.* **36**, 100772 (2020).
18. Marozas, J. A. et al. Wavelength-detuning cross-beam energy transfer mitigation scheme for direct drive: modeling and evidence from National Ignition Facility implosions. *Phys. Plasmas* **25**, 056314 (2018).
19. Bates, J. W. et al. Mitigation of cross-beam energy transfer in inertial-confinement-fusion plasmas with enhanced laser bandwidth. *Phys. Rev. E* **97**, 061202 (2018).
20. Froula, D. H. et al. A future of inertial confinement fusion without laser-plasma instabilities. *Phys. Plasmas* **32**, 052713 (2025).
21. Skupsky, S. et al. Improved laser-beam uniformity using the angular dispersion of frequency-modulated light. *J. Appl. Phys.* **66**, 3456–3462 (1989).
22. Craxton, R. S. et al. Direct-drive inertial confinement fusion: a review. *Phys. Plasmas* **22**, 110501 (2015).
23. Rothenberg, J. E. Comparison of beam-smoothing methods for direct-drive inertial confinement fusion. *J. Opt. Soc. Am. B* **14**, 1664–1671 (1997).
24. Hamadani, S. M. et al. Laser plasmas. *Appl. Phys. B* **29**, 186–188 (1982).
25. Rose, H. A. & DuBois, D. F. Initial development of ponderomotive filaments in plasma from intense hot spots produced by a random phase plate. *Phys. Fluids B Plasma Phys.* **5**, 3337–3356 (1993).
26. Raj, G. & Hüller, S. Impact of laser beam speckle structure on crossed beam energy transfer via beam deflections and ponderomotive self-focusing. *Phys. Rev. Lett.* **118**, 055002 (2017).
27. Hüller, S., Raj, G., Rozmus, W. & Pesme, D. Crossed beam energy transfer in the presence of laser speckle ponderomotive self-focusing and nonlinear sound waves. *Phys. Plasmas* **27**, 022703 (2020).
28. Barth, I. & Fisch, N. J. Reducing parametric backscattering by polarization rotation. *Phys. Plasmas* **23**, 102106 (2016).
29. Zhou, H. Y. et al. Kinetic simulation of nonlinear stimulated raman scattering excited by rotated polarized pump. *Plasma Phys. Control. Fusion* **61**, 105004 (2019).
30. Liu, Z. J. et al. Faraday effect on stimulated raman scattering in the linear region. *Plasma Phys. Control. Fusion* **60**, 045008 (2018).
31. Ma, H. H. et al. Mitigating parametric instabilities in plasmas by sunlight-like lasers. *Matter Radiat. Extrem.* **6**, 055902 (2021).
32. Xiong, H., Wu, S., Zhong, Z. & Zhang, B. Beam smoothing and polarization randomizing using quasi-broadband laser. *Opt. Commun.* **548**, 129819 (2023).
33. Aasi, J., Abbott, B. P., Abbott, R. et al. Advanced ligo. *Class. Quantum Gravity* **32**, 074001 (2015).
34. Ganapathy, D., Jia, W., Nakano, M. et al. Broadband quantum enhancement of the ligo detectors with frequency-dependent squeezing. *Phys. Rev. X* **13**, 041021 (2023).
35. Kozlov, V. A., Hernández-Cordero, J. & Morse, T. F. All-fiber coherent beam combining of fiber lasers. *Opt. Lett.* **24**, 1814–1816 (1999).
36. Stark, H. et al. Electro-optically controlled divided-pulse amplification. *Opt. Express* **25**, 13494–13503 (2017).

37. Laboratory for Laser Energetics. Flux: a next-generation broadband laser for direct-drive fusion experiments. Accessed 2026. https://www.lle.rochester.edu/publications/flux-a-next-generation-broadband-laser-for-direct-drive-fusion-experiments/ (2026).
38. Myatt, J. F. et al. A wave-based model for cross-beam energy transfer in direct-drive inertial confinement fusion. *Phys. Plasmas* **24**, 056308 (2017).
39. Myatt, J. F. et al. Lpse: A 3-d wave-based model of cross-beam energy transfer in laser-irradiated plasmas. *J. Comput. Phys.* **399**, 108916 (2019).
40. Williams, E. A. et al. The frequency and damping of ion acoustic waves in hydrocarbon (CH) and two-ion-species plasmas. *Phys. Plasmas* **2**, 129–138 (1995).
41. Stokes, G. G. in (Trans. Cambridge Philos. Soc., 9:339-412, 1852).
42. Collett, E. in (Marcel Dekker, New York, 1993).
43. Seaton, A. G., Yin, L., Follett, R. K., Albright, B. J. & Le, A. Cross-beam energy transfer in direct-drive icf. ii. theory and simulation of mitigation through increased laser bandwidth. *Phys. Plasmas* **29**, 042707 (2022).
44. Dawson, J. M. Particle simulation of plasmas. *Rev. Mod. Phys.* **55**, 403–447 (1983).
45. Fryxell, B. et al. Flash: An adaptive mesh hydrodynamics code for modeling astrophysical thermonuclear flashes. *Astrophys. J. Suppl. Ser.* **131**, 273 (2000).

Acknowledgements

This work employed the LPSE code developed with support from the Department of Energy National Nuclear Security Administration under Award Number DE-NA0004144 and the U.S. Department of Energy (DOE), Office of Science, Fusion Energy Sciences, under Award No. DE-SC0024863: IFE-STAR. This report was prepared as an account of work sponsored by an agency of the United States Government. Neither the United States Government nor any agency thereof, nor any of their employees, makes any warranty, express or implied, or assumes any legal liability or responsibility for the accuracy, completeness, or usefulness of any information, apparatus, product, or process disclosed, or represents that its use would not infringe privately owned rights. Reference herein to any specific commercial product, process, or service by trade name, trademark, manufacturer, or otherwise does not necessarily constitute or imply its endorsement, recommendation, or favoring by the United States Government or any agency thereof. The views and opinions of authors expressed herein do not necessarily state or reflect those of the United States Government or any agency thereof.

Author contributions

G.R. conducted the numerical simulations, analyzed the results, and wrote the manuscript with inputs from A.S., T.C., S.G., R.K.F., P.M.P., P.R., and S.N. The numerical simulation code was provided by R.K.F.

Competing interests

G.R., A.S., T.C., S.G., P.M.P., P.R. and S.N. are employees of Blue Laser Fusion Inc. R.K.F. declares no competing interests.

Additional information

Correspondence and requests for materials should be addressed to G. Raj.

Peer review information *Communications Physics* thanks Suming Weng and Yao Zhao for their contribution to the peer review of this work.

Reprints and permissions information is available at http://www.nature.com/reprints

Publisher's note Springer Nature remains neutral with regard to jurisdictional claims in published maps and institutional affiliations.

Open Access This article is licensed under a Creative Commons Attribution 4.0 International License, which permits use, sharing, adaptation, distribution and reproduction in any medium or format, as long as you give appropriate credit to the original author(s) and the source, provide a link to the Creative Commons licence, and indicate if changes were made. The images or other third party material in this article are included in the article's Creative Commons licence, unless indicated otherwise in a credit line to the material. If material is not included in the article's Creative Commons licence and your intended use is not permitted by statutory regulation or exceeds the permitted use, you will need to obtain permission directly from the copyright holder. To view a copy of this licence, visit http://creativecommons.org/licenses/by/4.0/.

© The Author(s) 2026

This Article in Press is shared early to give you faster access to new research. It is citable and carries a permanent DOI. The final edited version will replace it automatically.